Source-Independent Zone-1 Protection for Converter-Dominated Power Networks

Subhadeep Paladhi, Jaisaikiran Reddy Kurre and Ashok Kumar Pradhan, *Senior Member, IEEE*

***Abstract*—Growing penetration of converter-interfaced renewable energy sources with numerous control operations results in non-homogeneous fault characteristics in the network. Distance relay Zone-1 operation with such non-homogeneous situation may be vulnerable compromising both dependability and security aspects. In this work, vulnerability analysis is carried out to identify the factors influencing Zone-1 performance in a renewable integrated power network, and a method is proposed to ensure its correct operation. The method considers the homogeneity present in negative and zero sequence networks with converter-based sources to obtain the faulted loop current angle using local measurements and to derive correct decisions. The proposed method is tested for different renewable integrated systems, even with 100% converter-based sources and with variations in different vulnerable factors. Comparison with available distance relaying techniques demonstrates the superior performance of the proposed method.**

***Index Terms*—Renewable integrated power network, power network faults, distance relay, Zone-1 protection.**

I. Introduction

A. Motivation

POWER grids are experiencing a rapid growth in converter-interfaced renewable energy sources (CIRES) to meet the ambitious decarbonization target [1]–[3]. Reliable power system operation meeting the grid code requirements compels the control operations of the converters, interfacing such sources, to adjust accordingly [4]. Grid-forming controls are now being introduced in the converters to provide a stable grid operation with high renewable penetration [5], [6]. Large renewable plants connected to transmission networks are complied with fault ride through capability [7], [8]. Thus, numerous control actions associated with the converters influence the fault characteristics in the network differently compared to the system with only synchronous generators, which introduces non-homogeneity in the system with the modulation of equivalent impedances of the renewable plants. Generation variability and fault current limitation also influence the source-impedance-ratio (SIR) for the distance relay at renewable connected bus. These factors impel to reevaluate distance relay performance for the networks with high penetration of renewable sources.

B. Literature Review

Converter control operations and the generation variability with CIRESs influence the performance of distance relay, used commonly for network protection [9]–[13]. Techniques proposed for distance relay performance improvement in such a situation can be divided into different categories, which are described in this section with their limitations.

1) Decision with multiple settings: Distance relays with fixed zone settings often underreach for high SIRs. Multiple boundary settings may be available in a distance relay for different SIRs [14]–[17]. High penetration of CIRESs changes system dynamics rapidly. Instantaneous update in relay setting, required for primary protection in dynamic system condition, is difficult to achieve with such a scheme. Further, distance relays with large fault resistance coverage are prone to load encroachment, especially in high SIR situations [17].

2) Adaptive setting based approaches: Adaptive techniques are available in [9], [11] to set distance relays protecting lines connecting wind plants. Information (like plant and weather status) obtained through communication links are employed in those methods, which may delay the protection decision. Adaptive Zone-1 setting techniques based on local data are proposed in [18], [19] for stressed system conditions following structural and operational changes. The techniques requiring source equivalent estimation are not evaluated with CIRESs.

3) Data Driven Approaches: Distance relays, set with data driven approaches, may compensate the effect of high fault resistance [20], [21]. Converter control operation diversity and generation variability associated with renewable sources compel such techniques to be under scrutiny. In addition, the requirement of a large number of training data sets in such approaches restrains their application in real power systems.

4) Communication assisted schemes: Communication based trip schemes are recommended in [22], [23] for lines connecting CIRESs. Such schemes may also fail to ensure correct protection decision, when an internal fault is seen outside the zone boundary for both end relays. In addition, the latency associated with trip-command-transfer delays the decision obtained by such schemes.

5) Modification in Control schemes: Fault current characteristic of a synchronous generator is imitated in [24] by suitable modification in CIRES control scheme. Diversity in control operation with different CIRESs creates difficulty in generalizing such an approach.

6) Other Approaches: Fault resistance in the presence of infeed current from the remote end affects the distance relay performance. Different adaptive techniques are available in [25]–[27] to compensate such an affect, which consider either both end equivalent source impedances to be negligible and/or the system to be homogeneous. Both considerations are not true for a CIRES integrated system. The adaptive distance relaying technique proposed in [12] for lines connecting CIRESs compensates the effect of fault resistance by estimating faulted path current angle using local data. The technique considers

The work is supported in part by the Central Power Research Institute, Bangalore, India, under Grant RSOP/2019/TR/07 and conducted at the Department of Electrical Engineering, Indian Institute of Technology, Kharagpur, India (e-mail:paladhisubha91@gmail.com).

This is a peer reviewed, accepted author manuscript of the following research article: PALADHI, S., Kurre, J. R., & Pradhan, A. K. (2022). Source-Independent Zone-1 Protection for Converter-Dominated Power Networks. IEEE Transactions on Power Delivery. https://doi.org/10.1109/TPWRD.2022.3218615

the magnitude of grid impedance to be very small compared to line and renewable plant impedances. Such a consideration is not valid for weak grid conditions, especially with high penetration of CIRESs in the grid. A delayed decision is recommended in [13] for the relay at CIRES connected substation. In addition to the time issue, performance of such an approach is affected by incorrect operation of the remote end relay. In order to overcome such limitations with the available techniques, a new protection method is being sought for the power networks with growing renewable penetration.

C. Contribution

In this work, a vulnerability analysis is carried out to identify the factors affecting Zone-1 distance relay performance in the presence of converter-based sources. Thereafter a method is proposed to ensure correct protection operation. The method analyzes sequence networks individually and identifies the homogeneity present in negative and zero sequence networks with CIRESs. Applying this property, the method obtains the faulted loop current angle using local voltage and current measurements and derives correct decisions. Thus the method provides a generalized Zone-1 protection approach, which can be applied for power networks with and without converter-based sources. Performance of the proposed method is tested for a CIRES integrated 39-bus system and a 9-bus system with 100% converter-based sources, with variation in different vulnerability factors like fault location, fault resistance, CIRES generation, grid code requirement, converter control operation and grid strength. Comparison with available distance relaying demonstrates the accurate and superior performance of the proposed method.

II. Zone-1 Vulnerability in the Presence of Converter-Interfaced Renewable Sources

A two bus equivalent renewable integrated power system is presented in Fig. 1. System equivalents at both ends of line MN without any CIRES are represented using voltage sources (E_{S1} and E_{R1}) with internal impedances (Z_{S1} and Z_{R1}). The grid following renewable sources connected at both ends of the line are presented using voltage dependent current sources (I_{RN1} and I_{RN2}) in parallel with variable impedances (Z_{RN1} and Z_{RN2}). Z_L represents the impedance of line MN. At times, the buses of Fig. 1 may be connected to only one type of source also depending on the system conditions and availability of sources. The system is simplified by converting

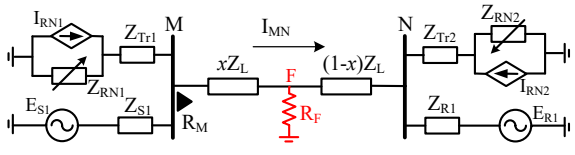

Fig. 1. Two bus equivalent model of renewable integrated power systems.

the current sources at both ends to equivalent voltage sources [28]. E_S and E_R with variable series impedances (Z_S and Z_R) in Fig. 2 represent the equivalent model of the systems connected at the corresponding end of line MN in Fig. 1. Z_S and Z_R vary with the control operations associated with renewable plants and their generation status.

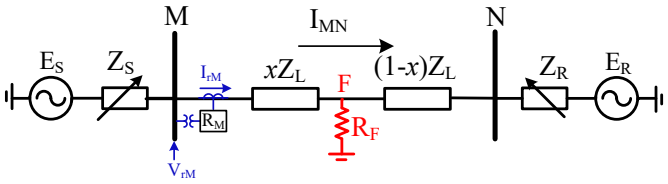

Fig. 2. Simplified model of Fig. 1.

Apparent impedance (Z_{app}) calculated by the distance relay R_M for a fault, created at a distance of x pu from bus M and with a fault resistance R_F, is given by [29],

$$Z_{app} = \frac{V^f_{rM}}{I^f_{rM}} = xZ_{1L} + \left(\frac{I_F}{I^f_{rM}}\right) R_F = xZ_{1L} + \Delta Z. \quad (1)$$

Where, V_{r_M} and I_{r_M} are the operating voltage and current for the relay, R_M. Faulted path current is represented by I_F. Superscript 'f' indicates the measurements during fault. V_r, I_r and I_F are different functions of voltages and currents in accordance to the fault type [12]. Subscript '1' indicates the positive sequence component.

For a 3-phase fault, $I_{rM} = I_{1M}$ and $I_F = I_{1F}$ [12]. Thus the additional impedance, ΔZ in (1) can be expressed as

$$\Delta Z = \left(\frac{I_{1F}}{I^f_{1M}}\right) R_F. \quad (2)$$

Using the superimposed property, I_{1M} during fault can be expressed as the summation of prefault current (I^{pre}_{1M}) and the incremental current (ΔI_{1M}), as in (3). Superscripts '*pre*' indicates the measurements during prefault.

$$I^f_{1M} = I^{pre}_{1M} + \Delta I_{1M} \quad (3)$$

Using (3), (2) can be rewritten as,

$$\Delta Z = \frac{R_F}{\left(\frac{I^{pre}_{1M}}{I_{1F}} + \frac{\Delta I_{1M}}{I_{1F}}\right)} \quad (4)$$

Pure-fault network of the system in Fig. 2 is presented in Fig. 3 [12]. Applying current distribution principle the relation between ΔI_{1M} and I_{1F} in Fig. 3 is expressed in (5).

$$\Delta I_{1M} = C_1 I_{1F} \quad (5)$$

where, $C_1 = \frac{(1-x)Z_{1L}+Z^{pf}_{1R}}{Z^{pf}_{1S}+Z_{1L}+Z^{pf}_{1R}}$. '*pf*' in superscript indicates the pure-fault impedance of the corresponding equivalent system.

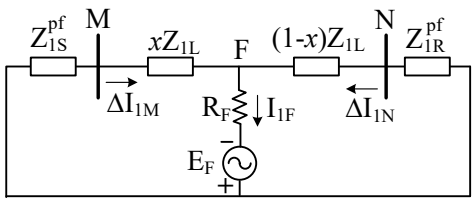

Fig. 3. Pure-fault model of the system in Fig. 2.

E_F in Fig. 3 is the voltage at F just prior to fault and can be obtained as,

$$E_F = V^{pre}_{1M} - xZ_{1L} I^{pre}_{1M} \quad (6)$$

Using (6), I_{1F} in Fig. 3 can be derived as in (7).

$$I_{1F} = \frac{V_{1M}^{pre} - xZ_{1L}I_{1M}^{pre}}{Z_{1T}^{pf} + R_F} \tag{7}$$

where, $Z_{1T}^{pf} = \frac{\left(Z_{1S}^{pf}+xZ_{1L}\right)\left((1-x)Z_{1L}+Z_{1R}^{pf}\right)}{Z_{1S}^{pf}+Z_{1L}+Z_{1R}^{pf}}$.
Using (5) and (7), ΔZ in (4) can be rewritten as,

$$\Delta Z = \frac{R_F}{\frac{Z_{1T}^{pf}+R_F}{\left(V_{1M}^{pre}/I_{1M}^{pre}\right)-xZ_{1L}} + C_1} \tag{8}$$

With similar approach ΔZ for other types of faults is derived in Appendix-I, which reveals ΔZ to be a function of several variables as in (9).

$$\Delta Z = f\left(V_{1M}^{pre}, I_{1M}^{pre}, Z_{(0,1,2)S}^{pf}, Z_{(0,1,2)R}^{pf}, Z_{(0,1,2)L}, x, R_F\right) \tag{9}$$

Subscripts '0' and '2' indicate the zero and negative sequence components respectively. A noticeable variation is observed for V_{1M}^{pre} and I_{1M}^{pre} in a high renewable penetrated system with change in generation status of CIRESs, especially at the buses connected to large renewable plants. Pure-fault impedances of converter-based sources vary significantly in accordance with their control operation depending on the fault severity. Equivalent system impedance without CIRESs also gets affected following any structural and operational changes in the system. Influence of such variations on distance relay performance is demonstrated for different fault cases created in a renewable integrated 39-bus system, as in Fig. 4. The renewable plants (solar and wind farms), connected at

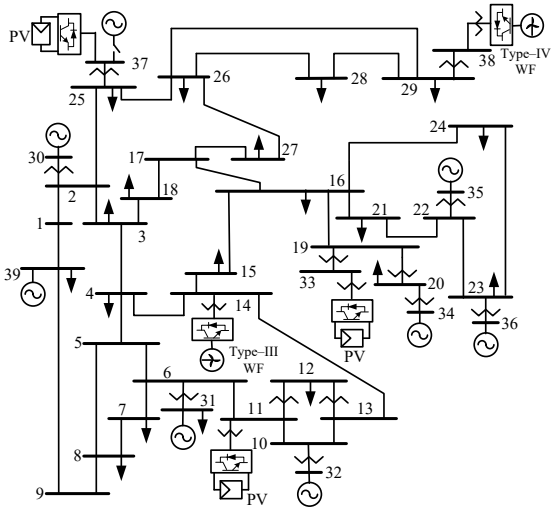

Fig. 4. 39-bus system integrating renewable sources.

bus 11, 14, 33, 37 and 38, are of 300 MVA each (detailed specifications of the plants are mentioned in Appendix-II). Solar plants are interfaced to grid through DC/AC inverter. For type-III wind farm, stator is directly connected to the grid and the rotor is connected through a back-to-back power electronic converter. Type-IV wind farm is connected to the grid through full-scale AC-DC-AC converter. Following such standard converter arrangement, each renewable plant is interfaced to the grid through a dYg type step-up transformer [30]–[32]. Grid-following converters interfacing the CIRESs are controlled in synchronous reference frame with feedforward compensation and generates balanced current even for asymmetrical faults satisfying dynamic reactive current requirement imposed by the applied grid code [4], [24]. The CIRESs follow the NERC reliability standard guidelines for fault-ride-through and internal protection [33].

Results in Fig. 5(a) demonstrate the performance of the relay at bus 25 for phase-B-to-phase-C-to-ground (BCG) faults created in line 25-2 at a distance of 50% from bus 25 for different R_F and solar plant generation at bus 37. The solar plant generation is maintained at 50% of its total capacity for the fault cases with different R_F, whereas the R_F is kept fixed at 15 Ω for the cases with different solar plant generation. It is observed that the faults created in Zone-1 may be seen in Zone-2 with variation in fault severity and solar plant generation. Sometime the apparent impedance calculated for Zone-1 fault is seen to remain outside the Zone-2 boundary. On the other hand, results in Fig. 5(b) demonstrate the performance of the relay at bus 2 for phase-A-to-ground (AG) faults created in line 25-26 at a distance of 10% from bus 25, for similar variation in R_F and solar plant generation, as considered for earlier case. Apparent impedances calculated for Zone-2 faults may be seen in Zone-1 or may remain outside the Zone-2 depending on R_F and system conditions. For both the cases, all CIRESs in the system operate with power factor between 0.95 lag to 0.95 lead even during fault, following the North American Grid Code (NAGC) [33]. Thus the distance relays may become vulnerable with both dependability and security aspects with high penetration of renewable sources in the system.

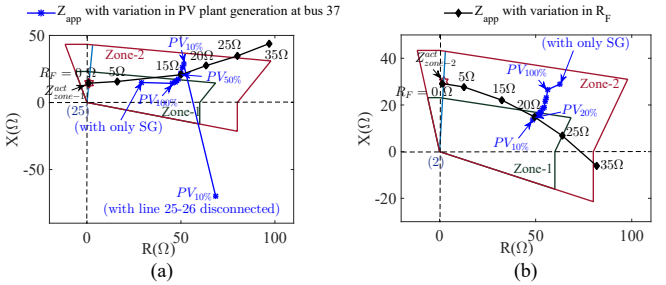

Fig. 5. Performance of distance relay for (a) Zone-1 and (b) Zone-2 faults with variation in R_F and solar plant generation at bus 37.

Such issues demand a source-independent protection solution to ensure correct distance relay decision in renewable integrated power systems.

III. Proposed Method for Reliable Distance Protection Decision

A new protection method is derived in this section using local voltage and current data to obtain correct distance relaying decision for Zone-1 faults in a renewable integrated power system.

Apparent impedance calculated by a distance relay in (1) is rewritten in (10) by expanding the variables with their complex forms.

$$\frac{\left|V_{rM}^{f}\right|}{\left|I_{rM}^{f}\right|}e^{j(\alpha-\beta)} = x|Z_{1L}|e^{j\theta_{1L}} + \frac{|I_F|}{\left|I_{rM}^{f}\right|}e^{j(\gamma-\beta)}R_F \tag{10}$$

α and β are the phase angles of V_{rM} and I_{rM}. θ_{1L} and γ represent the line impedance angle and the faulted path current phase respectively. (10) is rewritten in (11) by multiplying both sides of (10) by $e^{j(\beta-\gamma)}$.

$$\frac{\left|V^f_{rM}\right|}{\left|I^f_{rM}\right|}e^{j(\alpha-\gamma)} = x|Z_{1L}|e^{j(\theta_{1L}-\gamma+\beta)} + \frac{|I_F|}{\left|I^f_{rM}\right|}R_F \tag{11}$$

By separating the imaginary parts from both sides, (11) is rewritten in (12).

$$\frac{\left|V^f_{rM}\right|}{\left|I^f_{rM}\right|}\sin(\alpha-\gamma) = x|Z_{1L}|\sin(\theta_{1L}-\gamma+\beta) \tag{12}$$

Considering the range of x as $0 < x \leq 0.8$ for Zone-1 faults, two conditions are derived from (12), which are as follows.

$$\frac{D_1}{D_2} > 0 \quad \text{and} \quad \frac{D_1}{D_2} \leq 1 \tag{13}$$

where

$$\begin{aligned} D_1 &= \frac{\left|V^f_{rM}\right|}{\left|I^f_{rM}\right|}\sin(\alpha-\gamma) \\ D_2 &= 0.8|Z_{1L}|\sin(\theta_{1L}-\gamma+\beta). \end{aligned} \tag{14}$$

θ_{1L} in (14) is known from the line impedance data. α and β are obtained from the measurements. Therefore, the computation of γ is the only requirement to derive correct protection decision for Zone-1 faults using the conditions in (13). Methods to compute γ for different fault types are provided in the following subsections. Sequence networks of a CIRES integrated transmission system for different fault types are presented in Fig. 6. Feed-forward compensation provided in CIRES control scheme generates balanced current even during asymmetrical faults. Therefore the negative sequence model of CIRES is represented with an open switch. The switch is considered to be closed when the CIRES is complied with a grid code requiring negative sequence current injection to the grid [34].

A. For AG fault

Applying Kirchoff's voltage law (KVL) in the faulted loop of Fig. 6(a), a relation can be derived as in (15).

$$V^f_{AM} - xZ_{1L}\left(I^f_{AM} + K_0 I^f_{0M}\right) - 3R_F I_{0F} = 0 \tag{15}$$

where, $K_0\left(=\frac{Z_{0L}-Z_{1L}}{Z_{1L}}\right)$ is the zero sequence compensation factor. From (15), the apparent impedance calculation for such a fault type is derived as,

$$\frac{V^f_{AM}}{I^f_{AM}+K_0 I^f_{0M}} = xZ_{1L} + \frac{3I_{0F}}{I^f_{AM}+K_0 I^f_{0M}}R_F. \tag{16}$$

Comparing the terms in (16) with (1), the following relations are obtained for AG faults.

$$V^f_{rM} = V^f_{AM},\ I^f_{rM} = \left(I^f_{AM} + K_0 I^f_{0M}\right),\ I_F = 3I_{0F} \tag{17}$$

Thus the phase angles required for protection decision using (13) are derived as in (18).

$$\alpha = arg(V^f_{AM}),\ \beta = arg\left(I^f_{AM}+K_0 I^f_{0M}\right),\ \gamma = arg(3I_{0F}) \tag{18}$$

dYg type connection in the main transformers connecting CIRESs to the grid isolates the zero sequence network from the CIRES control dynamics and maintain homogeneity as with conventional sources. Thus γ in (18) can be calculated using local zero sequence current as in (19).

$$\gamma = arg(3I_{0F}) = arg(I^f_{0M}) \tag{19}$$

B. For BC fault

Applying KVL in the faulted loop of Fig. 6(b), a relation for BC fault can be derived as in (20).

$$\left(V^f_{1M} - V^f_{2M}\right) - xZ_{1L}\left(I^f_{1M} - I^f_{2M}\right) + 2R_{ph}I_{2F} = 0 \tag{20}$$

By rearranging the terms in (20), the relation for apparent impedance calculation for such a fault type is expressed as,

$$\frac{V^f_{1M} - V^f_{2M}}{I^f_{1M} - I^f_{2M}} = xZ_{1L} - \frac{2I_{2F}}{I^f_{1M} - I^f_{2M}}R_{ph}. \tag{21}$$

Comparing (21) with (1), the following relations are obtained for BC faults.

$$V^f_{rM} = \left(V^f_{1M}\text{–}V^f_{2M}\right),\ I^f_{rM} = \left(I^f_{1M}\text{–}I^f_{2M}\right),\ I_F = \text{–}2I_{2F} \tag{22}$$

Thus the phase angles required for protection decision using (13) are derived as in (23).

$$\alpha = arg\left(V^f_{1M}\text{–}V^f_{2M}\right), \beta = arg\left(I^f_{1M}\text{–}I^f_{2M}\right), \gamma = arg(\text{–}2I_{2F}) \tag{23}$$

A CIRES with feedforward compensation suppresses negative sequence current completely, whereas it emulates an apparent negative sequence reactance, largely similar to conventional synchronous generators when it is controlled to inject negative sequence current to the grid [35]. Thus, the negative sequence network in the presence of CIRESs remains homogeneous as with only having synchronous generator based sources. Therefore, γ in (23) can be calculated using local negative sequence current as in (24).

$$\gamma = arg(-2I_{2F}) = arg(I^f_{2M}) - \pi \tag{24}$$

If the local bus (M) is only connected to renewable plants, negative sequence current may not flow through bus M. In such a situation, I_{2F} becomes equal to the current flowing through the remote end (N). Negative sequence voltages at F and bus M are equal in such a situation. Considering homogeneity in the grid without CIRESs, Z_{2S2} can be expressed as a real-valued multiplier of Z_{2L} (i.e. $Z_{2S2} = K_2 Z_{2L}$) and I_{2F} can be obtained as in (25).

$$I_{2F} = -\frac{V^f_{2F}}{(1-x)Z_{2L} + Z_{2S2}} \approx -\frac{V^f_{2M}}{(1-x+K_2)Z_{2L}} \tag{25}$$

Thus γ in such a situation can be obtained as in (26).

$$\gamma = arg(-I_{2F}) = arg\left(\frac{V^f_{2M}}{Z_{2L}}\right) \tag{26}$$

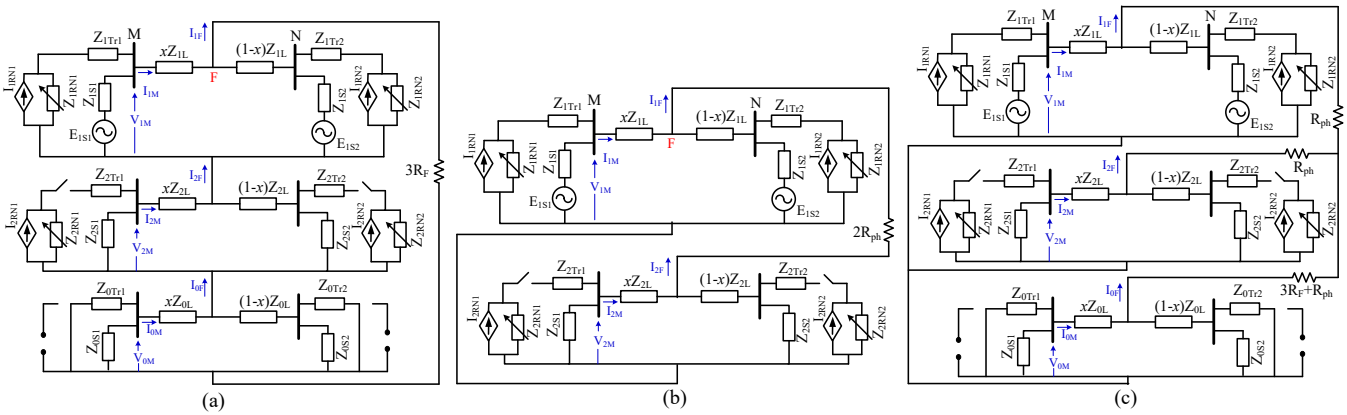

Fig. 6. Sequence networks of the system in Fig. 1 for (a) AG, (b) BC and (c) BCG faults.

C. For BCG fault

Applying KVL in the faulted loop of Fig. 6(c) (consisting of negative and zero sequence network), a relation can be derived as in (27).

$$\left(V^f_{2M}\text{–}V^f_{0M}\right) = xZ_{2L}\left(I^f_{2M}\text{–}K'_{0L}I^f_{0M}\right)\text{–}I_{0F}\left((1\text{–}m)\,R_{ph}\text{+}3R_F\right) \quad (27)$$

where, $K'_{0L} = \frac{Z_{0L}}{Z_{1L}}$ and $m = \frac{I_{2F}}{I_{0F}}$. Apparent impedance relation for BCG fault can be derived from (27) and expressed as in (28).

$$\frac{V^f_{2M}\text{–}V^f_{0M}}{I^f_{2M}\text{–}K'_0I^f_{0M}} = xZ_{1L}\text{–}\frac{I_{0F}}{I^f_{2M}\text{–}K'_{0L}I^f_{0M}}\left((1\text{–}m)\,R_{ph}\text{+}3R_F\right) \quad (28)$$

R_{ph} being the arcing resistance associated with phases is considered to be very small. It is negligible compared to $\mathrm{R_F}$ for high resistance faults. On the other hand, m becomes a real term for faults with low $\mathrm{R_F}$, due to homogeneity in the equivalent negative and zero sequence networks. Thus by comparing (28) with (1), the relations for BCG faults are obtained as follows.

$$V^f_{rM} = \left(V^f_{2M}\text{–}V^f_{0M}\right),\ I^f_{rM} = \left(I^f_{2M}\text{–}K'_0I^f_{0M}\right),\ I_F = \text{–}I_{0F} \quad (29)$$

Thus the phase angles required for protection decision using (13) for such a fault type can be obtained as in (30).

$$\begin{aligned}&\alpha = arg\left(V^f_{2M} - V^f_{0M}\right),\ \beta = arg\left(I^f_{2M} - K'_0I^f_{0M}\right),\\ &\gamma = arg(-I_{0F}) = arg(I^f_{0M}) - \pi\end{aligned} \quad (30)$$

D. For 3-phase (ABC) fault

For 3-phase faults, $V_{rM} = V_{1M}$ and $I_{rM} = I_{1M}$. The relation in (10) for such faults is rewritten in (31).

$$\frac{\left|V^f_{1M}\right|}{\left|I^f_{1M}\right|}e^{j(\alpha-\beta)} = x|Z_{1L}|e^{j\theta_{1L}} + \frac{|I_{1F}|}{\left|I^f_{1M}\right|}e^{j(\gamma-\beta)}R_F \quad (31)$$

By separating the imaginary parts from both sides, (31) is rewritten in (32).

$$\frac{\left|V^f_{1M}\right|}{\left|I^f_{1M}\right|}\sin(\alpha-\beta) = x|Z_{1L}|\sin\theta_{1L} + \frac{|I_{1F}|}{\left|I^f_{1M}\right|}\sin(\gamma-\beta)\,R_F \quad (32)$$

In (32), $|\sin(\gamma-\beta)| \leq 1$ and $\mathrm{R_F}$ for ABC fault is also small ($< 1\Omega$) [27]. Thus, the value of $\frac{|I_{1F}|}{\left|I^f_{1M}\right|}$ becomes insignificant when multiplied by $\sin(\gamma-\beta)\,R_F$ and (32) can be simplified, as in (33).

$$\frac{\left|V^f_{1M}\right|}{\left|I^f_{1M}\right|}\sin(\alpha-\beta) = x|Z_{1L}|\sin\theta_{1L} \quad (33)$$

Thus the indices D_1 and D_2 in (14) for such fault types are derived as in (34).

$$D_1 = \frac{\left|V^f_{1M}\right|}{\left|I^f_{1M}\right|}\sin(\alpha-\beta),\ D_2 = 0.8|Z_{1L}|\sin\theta_{1L} \quad (34)$$

E. Proposed relaying algorithm

Steps to be followed in the proposed protection approach are provided in Fig. 7. The scheme is initiated with fault detection. An undervoltage check is provided in addition to the usual overcurrent check for fault detection. Negative sequence component based checking is also applied in parallel to enhance the sensitivity for faults with high $\mathrm{R_F}$ [36]. Following the detection of a fault, it is classified using available local voltage measurements, as in [37]. Based on the fault type, relay calculates the indices D_1 and D_2 using (14) and (34). When $\left(\frac{D_1}{D_2}\right)$ is obtained in the range of $(0, 1]$ satisfying both the conditions in (13), the relay identifies the fault to be in Zone-1 and issues a trip decision.

IV. Results

Performance of the proposed method is evaluated for different faults created in the 39-bus system of Fig. 4. The proposed method is also tested for a 9-bus system with 100% renewable sources integrated through grid-following and grid-forming converters. A total number of 4550 faults are created for the evaluation, with variation in different influencing factors like fault location, fault resistance, renewable generation, grid strength, converter control operation with different renewable plants and grid codes. Applying the relation available in [38], the method is found to be 99.3% reliable. Results obtained for some of those cases are provided in this section.

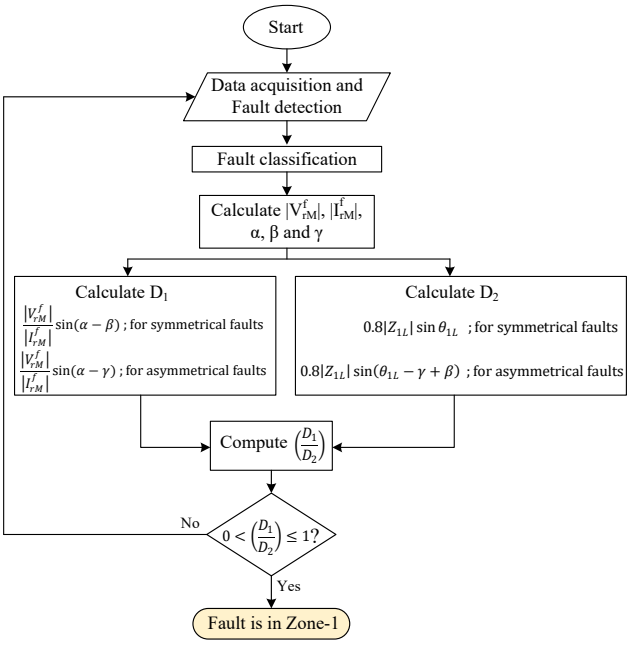

Fig. 7. Flow diagram of the proposed protection scheme.

A. For faults at different locations

Severity of a fault varies with its location from the relay bus and it influences the control operation of the renewable plants accordingly. Distance relay performance is affected significantly by the CIRESs, close to the faulted line. Performance of the relay at bus 25 is tested for BCG faults created at different locations in line 25-2, 25-26 and 2-3 with $R_F = 15\ \Omega$. Results in Fig. 8(a) demonstrate large differences between the apparent impedances calculated by the conventional distance relay and the actual faulted line section impedances. It is observed that the relay may find Zone-1 faults in Zone-2 and malfunction at times. The proposed method calculates two indices using (14) and checks the conditions, as in (13). Results in Fig. 8(b) demonstrate that $\left(\frac{D_1}{D_2}\right)$ calculated by the relay for all the faults created in line 25-26 is within the range (0,1], which confirm the faults to be in Zone-1. $\left(\frac{D_1}{D_2}\right)$ is obtained as negative for the fault created in line 25-26 (in the reverse direction), whereas it is calculated as greater than 1 for the Zone-2 fault created in line 2-3. Thus the proposed method ensures correct Zone-1 performance for faults at different locations. Results in Fig. 8(b) demonstrate that the proposed method can take correct decision within 1 cycle following fault inception, which satisfies the requirement of Zone-1 protection.

B. For faults with different fault resistances

Increase in fault resistance magnifies the effect of infeed current on conventional distance relay performance and deviates the apparent impedance significantly from the actual faulted section impedance in R-X plane. The nature of this deviation depends on the both end current angles, which is modulated by the control operation of the connected renewable plants. Results for two cases are presented in Fig. 9 demonstrating the influence of $\mathrm{R_F}$ on conventional and proposed methods. In the first case, performance of the distance relay at bus 25 is tested for BCG faults created in line 25-2 at a distance of 50% from bus 25 with different R_F, varying from 0 Ω to 35 Ω. On the other hand, the performance of the relay at bus 2 is tested for AG faults created in line 25-26 at a distance of 10% from bus 25 for similar $\mathrm{R_F}$ variations. Solar plant connected at bus 37 is considered to generate 50% of its total generation capacity for both the cases. Results in Fig. 9(a) demonstrate that faults created in Zone-1 may be seen in Zone-2 or faults created in Zone-2 may be seen in Zone-1 by the conventional distance relay. In some cases the apparent impedances are found to lie even outside Zone-2 boundary. Thus the relay possesses both security and dependability issues with variation in $\mathrm{R_F}$. As shown in Fig. 9(b), relay using proposed method calculates $\left(\frac{D_1}{D_2}\right)$ within the range (0,1] for all Zone-1 faults, whereas it is calculated higher than 1 for all the faults created in Zone-2. Thus the variation in $\mathrm{R_F}$ does not affect the robustness of the proposed method.

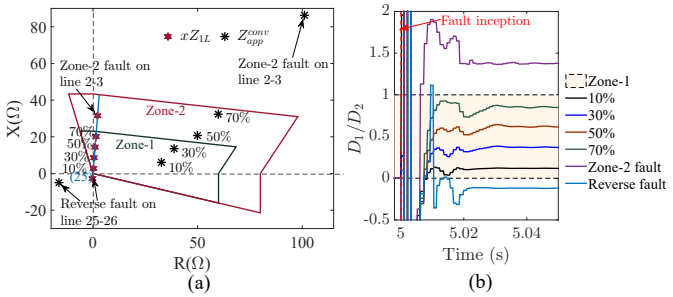

Fig. 8. Performance of distance relay for faults at different locations using (a) conventional and (b) proposed approaches.

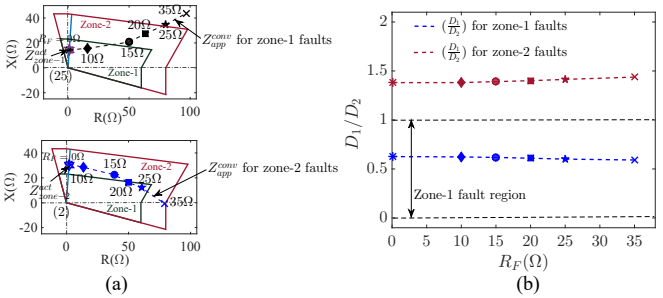

Fig. 9. Performance of distance relay for faults with different $\mathrm{R_F}$ using (a) conventional and (b) proposed approaches.

The proposed method is also tested at bus 25 for all types of faults created at different locations with variation in R_F. $\left(\frac{D_1}{D_2}\right)$ for some of those cases are provided in Table I. The Zone-1 faults are created in the middle of line 25-26, faults in Zone-2 are created in line 2-3 at a distance of 20% from bus 2 and faults in reverse direction are created in line 25-26 at a distance of 10% from bus 25. Results provided in Table I demonstrates that $\left(\frac{D_1}{D_2}\right)$ is obtained within (0,1] for Zone-1 faults, it is > 1 for Zone-2 faults and < 0 for faults in reverse direction. Thus, the proposed method derives correct protection decision for all types of faults with variation in $\mathrm{R_F}$.

C. For faults with change in renewable plant generation

Generation variability in the renewable plants near the relay bus affects the pre-fault voltage and current significantly and influences distance relay performance accordingly. In addition,

TABLE I
PERFORMANCE EVALUATION FOR DIFFERENT TYPES OF FAULTS

Fault Type	R_F (Ω)	Zone-1 fault in line 25-2	Zone-2 fault in line 2-3	Reverse fault in line 25-26
AG	0.1	0.63	1.38	-0.12
BG	10	0.63	1.40	-0.13
CG	100	0.64	1.45	-0.13
BC	0.1	0.63	1.50	-0.11
CA	1	0.62	1.45	-0.12
AB	5	0.61	1.38	-0.14
BCG	0.1	0.63	1.43	-0.13
ABG	10	0.62	1.38	-0.12
CAG	100	0.57	1.31	-0.11
ABC	0.1	0.62	1.47	-0.12
	1	0.62	1.34	-0.13
	5	0.58	1.21	-0.13

change in renewable plant generation modifies the equivalent impedance of the plant and also modulates the pure-fault impedance based on the control operation in the present generation status. Two cases are presented to demonstrate the performance of distance relay in such a scenario. In the first case, BCG faults are created in line 25-2 at a distance of 50% from bus 25 with $R_F = 15\ \Omega$ and performance of relay at bus 25 is tested with variation in solar plant generation at bus 37. In the second case, AG faults with $R_F = 20\ \Omega$ are created in line 25-26 at a distance of 10% from bus 25 and the performance of relay at bus 2 is tested for similar generation variation in the solar plant at bus 37. Performance of conventional distance relays are provided in Fig. 10. Relays are observed to perform correctly when only synchronous generator is connected at bus 37, but both relays maloperate at times with solar plant integration. Dependability for Zone-1 faults and security for Zone-2 faults are found to be the main concern. Reduction in solar plant generation increases the plant equivalent impedance and influence the distance relay performances significantly. The proposed method calculates both the indices D_1 and D_2 for all the fault cases, as provided in Fig. 11(a). As shown in Fig. 11(b), $\left(\frac{D_1}{D_2}\right)$ is obtained positive and less than 1 for all Zone-1 faults, whereas it is found to be greater than 1 for Zone-2 faults. Other CIRESs present in the system being

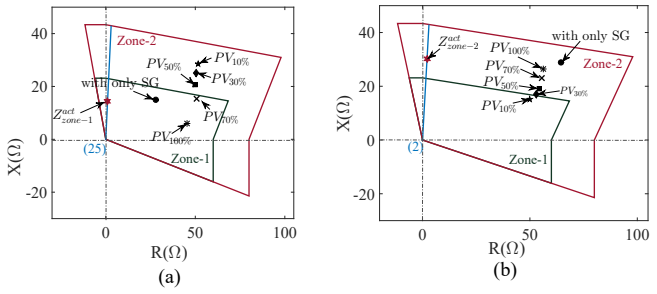

Fig. 10. Performance of distance relay with change in solar plant generation for(a) Zone-1 and (b) Zone-2 faults.

remotely connected do not influence much on the protection of line 25-2. In order to verify the influence of wind farm

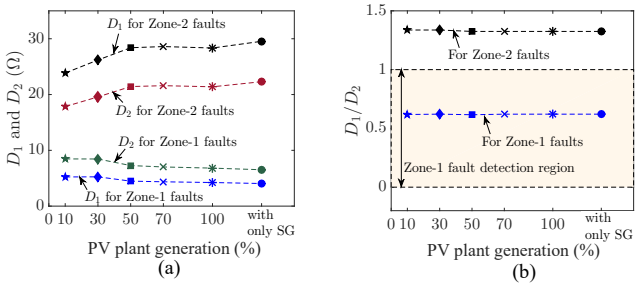

Fig. 11. Performance of the proposed method with change in solar plant generation: (a) D_1 and D_2, (b) (D_1/D_2).

generation variations on adjacent line protection, BCG faults (with $R_F = 15\ \Omega$) are created in line 14-4 and line 29-26 at a distance of 50% from bus 14 and 29 respectively, where the protection methods are tested. Generations at type-III and type-IV wind farms connected at bus 14 and 38 are varied for this study. Results provided in Fig. 11 demonstrate that the apparent impedance calculated by conventional distance relay varies significantly with change in generation of the adjacent wind farm and the relays fail to identify Zone-1 faults correctly in such situations. The relays with proposed method calculate $\left(\frac{D_1}{D_2}\right)$ for all the cases, which are provided in Table II. All the values satisfy both the conditions in (13) implying the faults to be in Zone-1. This demonstrates the proposed method to be independent of renewable plant generation adjacent to the protected line.

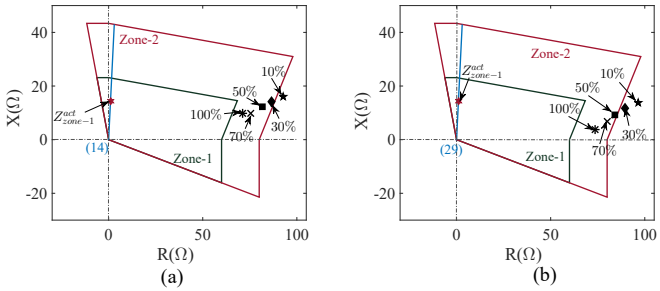

Fig. 12. Performance of distance relay for Zone-1 faults with change in generation of (a) type-III and (b) type-IV wind farms.

TABLE II
PERFORMANCE OF THE PROPOSED METHOD NEAR WIND FARMS

Relay Bus	Generation variation of adjacent CIRES				
	10%	30%	50%	70%	%100%
Bus 14	0.624	0.620	0.617	0.613	0.611
Bus 29	0.628	0.621	0.618	0.617	0.612

D. With change in grid code compliance of the adjacent renewable plant

Ratio between active and reactive fault current from a renewable plant changes with the grid code to satisfy the fault ride through requirements. Thus the fault current angle from a renewable plant is modulated with the change in grid code compliance. Such modulation influences conventional distance relay performance significantly. Two cases are presented here to demonstrated the performance of distance relays at bus 25 and 2, when the solar plant connected at bus 37 is complied

with two different grid codes, one at a time. With the first one, the solar plant operates close to unity power factor (similar to NAGC). On the other hand, the solar plant interfacing converter prioritizes reactive current injection while complied with the second one (as followed in European Union grid code (EU-GC)) [4], [24]. Results in Fig. 13(a) demonstrate the performance of distance relay at bus 25 for BCG faults created in line 25-2 at a distance of 50% from bus 25 with $R_F = 15\ \Omega$. On the other hand, performance of distance relay at bus 2 is presented in Fig. 13(b) for AG faults, created in line 25-26 at a distance of 10% from bus 25 with $R_F = 20\ \Omega$. It is observed that the apparent impedance calculated by a distance relay varies significantly with change in grid code compliance and may results in maloperation at times. $\left(\frac{D_1}{D_2}\right)$ calculated by the proposed method for all the cases are shown in Fig. 14. Results demonstrate that both the conditions mentioned in the proposed method are satisfied correctly even with change in grid code compliance. Thus the performance of the proposed method remain unaffected when CIRESs connected in the system are complied with different grid codes.

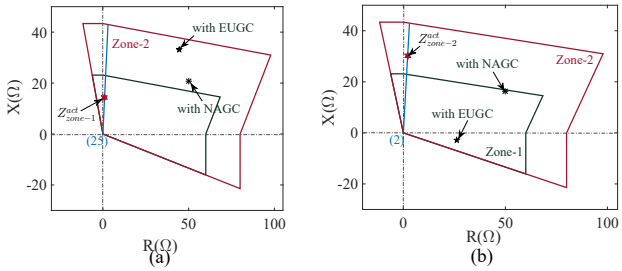

Fig. 13. Performance of distance relay with change in grid-code compliance in the adjacent renewable plant for (a) Zone-1 and (b) Zone-2 faults.

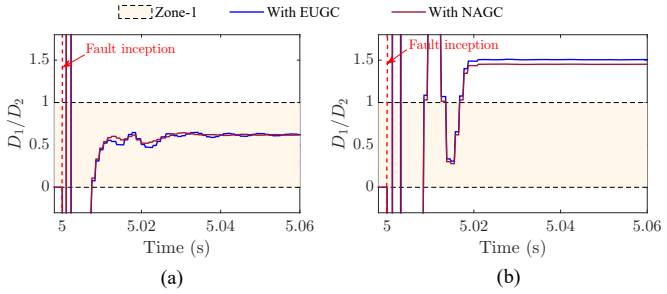

Fig. 14. Performance of the proposed method with change in grid-code with the adjacent renewable plant for (a) Zone-1 and (b) Zone-2 faults.

E. Performance evaluation for lines connecting only CIRES at the local end with different control schemes

Impact of converter-control operation becomes more prominent on protection decision when the relay bus is only connected to CIRESs. Considering line 25-26 to be out-of-operation, performance of distance relay and the proposed method is tested for such situations at bus 25 for BCG faults created in line 25-2 at a distance of 25% from bus 25 with $R_F = 25\Omega$. Impact of four different control operations is demonstrated in this study. The solar plant at bus 37 is replaced by a type-III and a type-IV wind farm, one at a time. All the CIRESs are controlled with balanced current controller and inject only positive sequence current even for asymmetrical faults. In addition, the methods are tested by incorporating negative sequence current injection capability in the solar plant. Results shown in Fig. 15(a) demonstrate that the apparent impedance calculated by distance relay varies significantly with change in control operation associated with the CIRES connected at the relay bus and results in relay maloperation. On the other hand, $\left(\frac{D_1}{D_2}\right)$ calculated for all those cases (as shown in Fig. 15(b)) are found to satisfy both the conditions in (13) ensuring correct Zone-1 protection decisions. This demonstrates the correct performance of the proposed method when the fault current at relay bus is only fed from CIRES and it is independent of control operation associated with the CIRES.

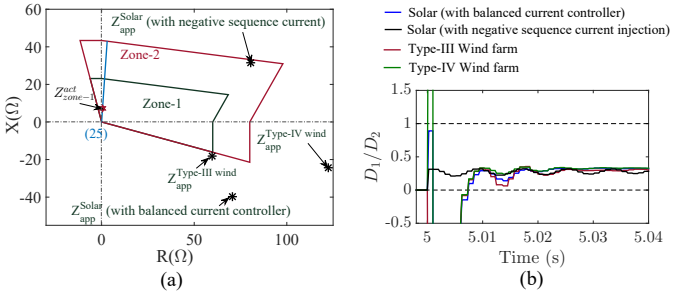

Fig. 15. Performance of (a) distance relay and (b) the proposed method for lines connecting only CIRES at the local end with different control schemes.

F. For a system with 100% converter-based sources and Comparative assessment

Performance of the proposed method is tested for a 9-bus system with 100% converter-based sources, as shown in Fig. 16 [39]. The solar plant connected at bus 2 is integrated to the grid through grid-following converter, whereas the solar plants at bus 1 and 3 are integrated through grid-forming converters. The grid-following converter operates with balanced current controller, as used in the previous case studies. On the other hand, grid-forming converters with dual-current controller are designed to mimic synchronous generator negative sequence impedance angle to maintain homogeneity as considered in Section-III.B. A BCG fault is created in line 7-8 at a distance of 50% from bus 7 with $R_F = 15\ \Omega$ and the performance of the distance relay at bus 7 is tested.

Results in Fig. 17 provides a comparative assessment with conventional distance relaying and the method available in [12]. As demonstrated in Fig. 17(a), the distance relay with conventional approach fails to find the fault within Zone-1 boundary due to the non-homogeneous fault response in the system. The method available in [12] considers the grid connected at remote end of the protected line to be strong with sufficient conventional synchronous generators, which is not true for a system, as considered here. Result in Fig. 17(b) shows a significant difference between the fault section impedance calculated using the method with the actual

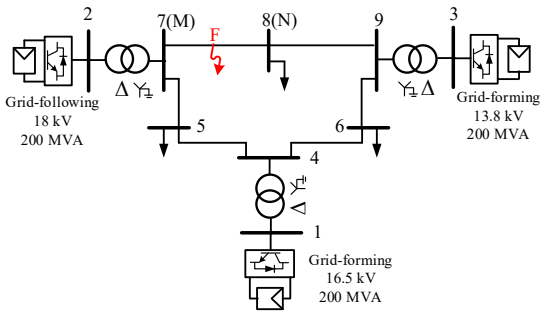

Fig. 16. 9-bus system with 100% converter-based sources.

and exposes its limited performance for converter-dominated power systems. On the other hand, the proposed method meets the criteria of (13), as shown in Fig. 17(c) and identifies the fault in Zone-1 correctly. This confirms the proposed method to be independent of system strength and sources with different control operations. It also reveals the necessity and advantages of the proposed method over conventional distance relaying and the method available in [12].

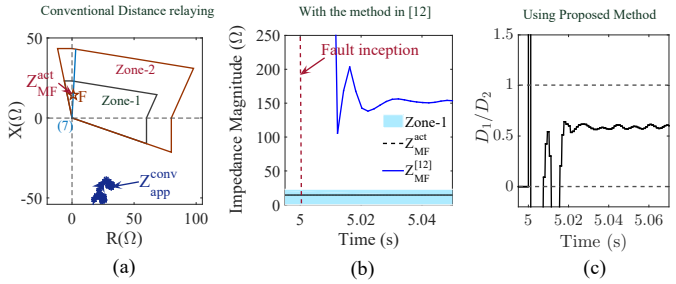

Fig. 17. Performances of (a) conventional distance relaying, (b) the method in [12] and (c) the proposed method for fault in a system with 100% converter-based sources.

The proposed protection method is compared with a few advanced distance relaying techniques proposed in recently available literature [12], [13], [40]–[42]. The comparative assessment is summarized in Table III. The table clearly depicts the advantages of the proposed method when compared to the other available techniques for converter-dominated power systems.

TABLE III
COMPARATIVE ANALYSIS WITH RECENT AVAILABLE METHODS

Parameters	Available Methods					Proposed Method
	[40]	[41]	[42]	[13]	[12]	
Applicable for all types of faults?	No	Yes	No	Yes	Yes	Yes
Applicable in weak grid condition?	Yes	No	Yes	No	No	Yes
Tested with high renewable penetration in grid?	No	No	No	No	No	Yes
Method independent of CIRES control scheme?	Yes	No	No	Yes	Yes	Yes
No requirement of remote end information?	Yes	Yes	Yes	No	Yes	Yes
Applicable to all buses in the system?	No	No	No	No	No	Yes

V. CONCLUSION

Fault characteristic modulation by converter-based sources influences distance relay performance in a renewable integrated power system significantly, and may result in maloperation at times. A vulnerability analysis is carried out to identify the factors affecting distance relay Zone-1 performance in such a situation. A generalized source-independent method is proposed to ensure correct Zone-1 operation. The method derives distance relay decision by estimating the faulted path current angle. Use of the homogeneity present in negative and zero sequence networks for the estimation ensures the accurate performance of the proposed method for any line in a power network with or without the connection of converter-based sources. The method does not require any additional information or measurement for its implementation. The improved performance of the proposed method is demonstrated for change in fault location, fault resistance, renewable plant generation, and grid code compliance of the CIRESs. Correct performance in a system with 100% converter-based sources validates the method to be independent of system strength and converter-control operation. Comparative assessment with available distance relaying techniques demonstrates the necessity and superiority of the proposed method in the new scenario of power grid operation.

APPENDIX-I

ΔZ for different types of asymmetrical faults (AG, BC and BCG) are derived in this section using the Sequence networks provided in Fig. 6.

A. For AG fault

The relay operating current for AG fault is expressed as,

$$I^f_{rM} = I^f_{AM} + K_0 I^f_{0M} = I^{pre}_{1M} + \Delta I_{1M} + I^f_{2M} + (1+K_0)\, I^f_{0M}. \quad (35)$$

Using the sequence network in Fig. 6 (a), the faulted loop current can be expressed as,

$$I_F = I_{1F} = I_{2F} = I_{0F} \quad (36)$$

Using (35) and (36), ΔZ in (1) can be expressed as,

$$\Delta Z = \frac{3R_F}{\left(\frac{I^{pre}_{1M}}{I_{1F}} + \frac{\Delta I_{1M}}{I_{1F}} + \frac{I^f_{2M}}{I_{2F}} + (1+K_0)\,\frac{I^f_{0M}}{I_{0F}}\right)}. \quad (37)$$

I_{1F} in Fig. 6 (a) can be obtained as,

$$I_{1F} = \frac{V^{pre}_{1M} - xZ_{1L} I^{pre}_{1M}}{Z^{pf}_{1T} + Z_{2T} + Z_{0T} + 3R_F}. \quad (38)$$

where,

$$Z_{2T} = \frac{(Z_{2S1} + xZ_{2L})\,((1-x)Z_{2L} + Z_{2S2})}{Z_{2S1} + Z_{2L} + Z_{2S2}}$$

$$Z_{0T} = \frac{((Z_{0Tr1} || Z_{0S1}) + xZ_{0L})\,((1-x)Z_{0L} + (Z_{0Tr2} || Z_{0S2}))}{(Z_{0Tr1} || Z_{0S1}) + Z_{0L} + (Z_{0Tr2} || Z_{0S2})}$$

Thus, ΔZ for AG fault can be derived as,

$$\Delta Z = \frac{R_F}{\frac{Z^{pf}_{1T} + Z_{2T} + Z_{0T} + 3R_F}{(V^{pre}_{1M}/I^{pre}_{1M}) - xZ_{1L}} + C_1 + C_2 + (1+K_0)\,C_0}. \quad (39)$$

where,

$$C_2 = \frac{(1-x)Z_{2L} + Z_{2S2}}{Z_{2S1} + Z_{2L} + Z_{2S2}}$$
$$C_0 = \frac{(1-x)Z_{0L} + (Z_{0Tr2}||Z_{0S2})}{(Z_{0Tr1}||Z_{0S1}) + Z_{0L} + (Z_{0Tr2}||Z_{0S2})}.$$

B. For BC fault

The relay operating current for BC fault is expressed as,

$$I^f_{rM} = I^f_{1M} - I^f_{2M} = I^{pre}_{1M} + \Delta I_{1M} - I^f_{2M}. \tag{40}$$

Using the sequence network in Fig. 6 (b), the faulted loop current can be expressed as,

$$I_F = I_{1F} - I_{2F} = 2I_{1F}. \tag{41}$$

Using (40) and (41), ΔZ in (1) can be rewritten as,

$$\Delta Z = \frac{2I_{1F}R_{ph}}{I^{pre}_{1M} + \Delta I_{1M} - I^f_{2M}}. \tag{42}$$

I_{1F} in Fig. 6 (b) can be obtained as,

$$I_{1F} = \frac{V^{pre}_{1M} - xZ_{1L}I^{pre}_{1M}}{Z^{pf}_{1T} + Z_{2T} + 2R_{ph}}. \tag{43}$$

Thus, ΔZ for BC fault is derived as,

$$\Delta Z = \frac{2R_{ph}}{\frac{Z^{pf}_{1T}+Z_{2T}+2R_{ph}}{\left(V^{pre}_{1M}/I^{pre}_{1M}\right)-xZ_{1L}} + C_1 - C_2}. \tag{44}$$

C. For BCG fault

The relay operating current for BCG fault is expressed as,

$$I^f_{rM} = I^f_{1M} - I^f_{2M} = I^{pre}_{1M} + \Delta I_{1M} - I^f_{2M}. \tag{45}$$

Using the sequence network in Fig. 6 (c), the faulted loop current for BCG fault can be expressed as,

$$I_F = I_{1F} - I_{2F}. \tag{46}$$

Applying current distribution property in Fig. 6 (c), I_{2F} can be expressed as,

$$I_{2F} = -D_2 I_{1F}. \tag{47}$$

where,

$$D_2 = \frac{Z_{0T} + R_{ph} + 3R_F}{Z_{2T} + Z_{0T} + 2R_{ph} + 3R_F}.$$

Using (45) and (46), ΔZ in (1) can be rewritten as,

$$\Delta Z = \frac{(1+D_2)\, I_{1F}R_{ph}}{I^{pre}_{1M} + \Delta I_{1M} - I^f_{2M}}. \tag{48}$$

I_{1F} in Fig. 6 (c) can be obtained as,

$$I_{1F} = \frac{V^{pre}_{1M} - xZ_{1L}I^{pre}_{1M}}{Z^{pf}_{1T} + R_{ph} + \frac{(Z_{0T}+R_{ph}+3R_F)(Z_{2T}+R_{ph})}{Z_{2T}+Z_{0T}+2R_{ph}+3R_F}}. \tag{49}$$

Thus, ΔZ for BCG fault can be derived as,

$$\Delta Z = \frac{(1+D_2)\, R_{ph}}{\frac{Z^{pf}_{1T}+R_{ph}+\frac{\left(Z_{0T}+R_{ph}+3R_F\right)\left(Z_{2T}+R_{ph}\right)}{Z_{2T}+Z_{0T}+2R_{ph}+3R_F}}{\left(V^{pre}_{1M}/I^{pre}_{1M}\right)-xZ_{1L}} + C_1 - C_2}. \tag{50}$$

TABLE IV
SIMULATION PARAMETERS OF CIRESS CONNECTED TO THE SYSTEM

Plant	Specifications
Solar Plant	Unit Capacity: 1 MVA; Total number of units: 300 Current Controller: K_P = 0.15 & T_i = 0.08 s Rated DC bus voltage: 600 V DC Link capacitor: 7800 μF Filter: L_f = 300μH, C_f= 200μF, R_f = 0.025Ω
Type-III Wind Farm	Unit capacity: 5 MVA; Total number of units: 60 Machine terminal voltage: 0.69 kV Converter reactor: 134 mH C_f = 700μF, C_{damp} = 300μF, L_{damp} = 620 mH, R_{damp} = 1.33 Ω, DC crowbar on voltage: 2.2 kV DC chopper activation voltage = 1.7 kV DC chopper Off voltage = 1.5 kV Shunt resistor: 1.2 Ω
Type-IV Wind Farm	Unit capacity: 5 MVA; Total number of units: 60 Machine terminal voltage: 0.69 kV Converter reactor: 200 μH VSC DC voltage set point = 1.45 kV Maximum reactive power = 0.3 pu Filter: C_f = 1000μF, C_{damp} = 500μF, L_{damp} = 1 mH, R_{damp} = 1 Ω

APPENDIX-II

REFERENCES

[1] "Renewables integration in india," NITI Ayog, International Energy Agency, Tech. Rep., April 2021, [Online]. Available: https://iea.blob.core.windows.net/assets/7b6bf9e6-4d69-466c-8069-bdd26b3e9ed1/RenewablesIntegrationinIndia2021.pdf.

[2] H. Lund and B. V. Mathiesen, "Energy system analysis of 100% renewable energy systemsthe case of denmark in years 2030 and 2050," *Energy*, vol. 34, no. 5, pp. 524–531, 2009.

[3] "Green energy corridors-II: (Part-A)," Power Grid Corporation of India Ltd., Tech. Rep., [Online]. Available: https://www.powergrid.in/sites/default/files/footer/smartgrid/Green%20Energy%20Corridor%202-Part%20A.pdf.

[4] IRENA, "Grid codes for renewable powered systems," International Renewable Energy Agency, Abu Dhabi, Tech. Rep., April 2022.

[5] W. Du, F. K. Tuffner, K. P. Schneider, R. H. Lasseter, J. Xie, Z. Chen, and B. Bhattarai, "Modeling of grid-forming and grid-following inverters for dynamic simulation of large-scale distribution systems," *IEEE Transactions on Power Delivery*, vol. 36, no. 4, pp. 2035–2045, 2021.

[6] ESIG, "Grid-forming technology in energy systems integration," Energy Systems Integration Group, Tech. Rep., March 2022.

[7] H. M. Hasanien, "An adaptive control strategy for low voltage ride through capability enhancement of grid-connected photovoltaic power plants," *IEEE Trans. Power Syst.*, vol. 31, no. 4, pp. 3230–3237, July 2016.

[8] Y. Wang and B. Ren, "Fault ride-through enhancement for grid-tied PV systems with robust control," *IEEE Trans. Ind. Electr.*, vol. 65, no. 3, pp. 2302–2312, March 2018.

[9] A. K. Pradhan and G. Joos, "Adaptive distance relay setting for lines connecting wind farms," *IEEE Trans. Energy Conv.*, vol. 22, no. 1, pp. 206–213, March 2007.

[10] A. Hooshyar, M. A. Azzouz, and E. F. El-Saadany, "Distance protection of lines emanating from full-scale converter-interfaced renewable energy power plants; part I: Problem statement," *IEEE Trans. Power Del.*, vol. 30, no. 4, pp. 1770–1780, Aug 2015.

[11] K. E. Arroudi and G. Joos, "Performance of interconnection protection based on distance relaying for wind power distributed generation." *IEEE Trans. Power Del.*, vol. PP, no. 99, pp. 1–1, 2017.

[12] S. Paladhi and A. K. Pradhan, "Adaptive distance protection for lines connecting converter-interfaced renewable plants," *IEEE J. Emerg. and Sel. Topics Power Electron.*, vol. 9, no. 6, pp. 7088–7098, 2021.

[13] Y. Fang, K. Jia, Z. Yang, Y. Li, and T. Bi, "Impact of inverter-interfaced renewable energy generators on distance protection and an improved scheme," *IEEE Trans. Ind. Electr.*, vol. 66, no. 9, pp. 7078–7088, Sep. 2019.
[14] M. Thompson and A. Somani, "A tutorial on calculating source impedance ratios for determining line length," in *Proc. 68th Annual Conference for Protective Relay Engineers*, March 2015, pp. 833–841.
[15] G. E. Alexander, J. G. Andrichak, and W. Z. Tyska, "Relaying short lines," GE Power Management, Tech. Rep., [Online]. Available: http://store.gedigitalenergy.com/faq/documents/alps/ger-3735.pdf.
[16] Siemens, "Distance protection relay for transmission lines," Tech. Rep., 1999, [Online]. Available: ftp://ftp.so-cdu.ru/RZA/Siemens/SIPROTEC
[17] Alstom, "Network protection and automation guide," Tech. Rep. 978-0-9568678-0-3, May 2011.
[18] S. Paladhi and A. K. Pradhan, "Adaptive zone-1 setting following structural and operational changes in power system," *IEEE Trans. Power Del.*, vol. 33, no. 2, pp. 560–569, April 2018.
[19] S. Paladhi and A. Pradhan, "Resilient protection scheme preserving system integrity during stressed condition," *IET Gen., Trans. Distr*, vol. 13, no. 14, pp. 3188–3194, 2019.
[20] K. Li, L. Lai, and A. David, "Stand alone intelligent digital distance relay," *IEEE Trans. Power Systems*, vol. 15, no. 1, pp. 137–142, Feb 2000.
[21] J. Upendar, C. Gupta, and G. Singh, "Comprehensive adaptive distance relaying scheme for parallel transmission lines," *IEEE Trans. Power Del.*, vol. 26, no. 2, pp. 1039–1052, April 2011.
[22] A. Hooshyar, M. A. Azzouz, and E. F. El-Saadany, "Distance protection of lines connected to induction generator-based wind farms during balanced faults," *IEEE Trans. Sustainable Energy*, vol. 5, no. 4, pp. 1193–1203, Oct 2014.
[23] A. Hooshyar, M. A. Azzouz, and E. F. El-Saadany, "Distance protection of lines emanating from full-scale converter-interfaced renewable energy power plants ; part II: Solution description and evaluation," *IEEE Trans. Power Del.*, vol. 30, no. 4, pp. 1781–1791, Aug 2015.
[24] A. Banaiemoqadam, A. Hooshyar, and M. A. Azzouz, "A control-based solution for distance protection of lines connected to converter-interfaced sources during asymmetrical faults," *IEEE Trans. Power Del.*, vol. 35, no. 3, pp. 1455–1466, 2020.
[25] Y. Liang, Z. Lu, W. Li, W. Zha, and Y. Huo, "A novel fault impedance calculation method for distance protection against fault resistance," *IEEE Trans. Power Del.*, vol. 35, no. 1, pp. 396–407, 2020.
[26] J. Ma, W. Ma, Y. Qiu, and J. Thorp, "An adaptive distance protection scheme based on the voltage drop equation," *IEEE Trans. Power Del.*, vol. 30, no. 4, pp. 1931–1940, Aug 2015.
[27] V. Makwana and B. Bhalja, "A new digital distance relaying scheme for compensation of high-resistance faults on transmission line," *IEEE Trans. Power Del.*, vol. 27, no. 4, pp. 2133–2140, Oct 2012.
[28] C. K. Alexander, *Fundamentals of Electric Circuits*. McGraw-Hill, 2009.
[29] G. Ziegler, *Numerical Distance Protection: Principles and Applications*. John Wiley & Sons, 2011.
[30] C. Loutan, P. Klauer, S. Chowdhury, S. Hall, M. Morjaria, V. Chadliev, N. Milam, C. Milan, and V. Gevorgian, "Demonstration of essential reliability services by a 300-MW solar photovoltaic power plant," National Renewable Energy Lab.(NREL), Golden, CO (United States), Tech. Rep., 2017.
[31] PSCAD, "Type 3 wind turbine model," Tech. Rep., November 2018.
[32] PSCAD, "Type 4 wind turbine model," Tech. Rep., December 2018.
[33] NERC, "Reliability guideline: Improvements to interconnection requirements for BPS-connected inverter-based resources," Atlanta, GA 30326, Tech. Rep., September 2018, [Online]. Available: https://www.nerc.com/comm/OC_Reliability_Guidelines_DL/Inverter-Based_Resource_Performance_Guideline.pdf.
[34] VDE-AR-N 4130, "Technical requirements for the connection and operation of customer installations to the extra high voltage network (TCR extra high voltage)," Tech. Rep., November 2018.
[35] M. Nagpal, M. Jensen, and M. Higginson, "Protection challenges and practices for interconnecting inverter based resources to utility transmission systems," Working Group C32, Power System Relaying and Control Committee, Tech. Rep., 2020.
[36] S. Paladhi and A. K. Pradhan, "Adaptive fault type classification for transmission network connecting converter-interfaced renewable plants," *IEEE Syst. J.*, vol. 15, no. 3, pp. 4025–4036, 2021.
[37] A. Hooshyar, E. F. El-Saadany, and M. Sanaye-Pasand, "Fault type classification in microgrids including photovoltaic DGs," *IEEE Trans. Smart Grid*, vol. 7, no. 5, pp. 2218–2229, Sept 2016.
[38] A. Zitouni, "Power transformer differential relay reliability assessment using false trip root cause analysis," in *International Conference on Electrical Engineering (ICEE)*, 2020, pp. 1–5.
[39] R. W. Kenyon, A. Sajadi, A. Hoke, and B.-M. Hodge, "Open-source PSCAD grid-following and grid-forming inverters and a benchmark for zero-inertia power system simulations," in *IEEE Kansas Power and Energy Conference (KPEC)*, 2021, pp. 1–6.
[40] Y. Liang, W. Li, and Y. Huo, "Zone i distance relaying scheme of lines connected to MMC-HVDC stations during asymmetrical faults: Problems, challenges, and solutions," *IEEE Trans. Power Del.*, vol. 36, no. 5, pp. 2929–2941, 2021.
[41] K. Ma, H. K. Hoidalen, Z. Chen, and C. L. Bak, "Improved zone 1 top-line tilting scheme for the polygonal distance protection in the outgoing line," *CSEE Journal of Power and Energy Systems*.
[42] C. Chao, X. Zheng, Y. Weng, Y. Liu, P. Gao, and T. Nengling, "Adaptive distance protection based on the analytical model of additional impedance for inverter-interfaced renewable power plants during asymmetrical faults," *IEEE Trans. Power Del.*, 2021, available in early access.

Subhadeep Paladhi received PhD degree in Electrical Engineering from Indian Institute of Technology, Kharagpur, India in 2021. He is currently working as a Research Associate in the Department of Electronic and Electrical Engineering, University of Strathclyde, Glasgow, U.K.

Jaisaikiran Reddy Kurre received M.Tech. degree in Electrical Engineering from Indian Institute of Technology, Kharagpur, India.

Ashok Kumar Pradhan is a Professor in the Department of Electrical Engineering, Indian Institute of Technology, Kharagpur, India. Prof. Pradhan is a Fellow of Indian National Academy of Engineering and the National Academy of Sciences, India.